JOURNAL OF MATERIALS SCIENCE 28 (1993) 2999–3013

Quantitative kinetic analysis of silicon nitridation

R. G. PIGEON, A. VARMA
Department of Chemical Engineering, University of Notre Dame, Notre Dame, IN 46556, USA

Kinetic analysis of silicon nitridation requires intrinsic single-particle behaviour to be isolated from global or compact effects that typically manifest during the reaction-bonding process. These effects arise from the influence of adjacent particles, which modify the macropore structure as the reaction proceeds. Much of the variation in the published kinetic data can be attributed to compact effects, particle shape, and size distribution, resulting in a myriad of models being reported, each only applicable to the nitridation conditions in which the data were obtained. Our work clearly demonstrates that the intrinsic single-particle nitridation behaviour is well described by a sharp-interface model, with diffusion control (E_a = 301.5–310.0 kJ mol^{-1}) through an expanding Si_3N_4 product layer developing on the individual grains. For the nitridation of silicon compacts, the reaction-bonding process can be divided into three fundamental stages: (1) initial devitrification/nucleation, (2) massive nitridation, and (3) termination by further sintering, densification, and coarsening of the Si_3N_4 product. Factors influencing and controlling each stage are summarized.

1. Introduction

The reaction between silicon and nitrogen to form silicon nitride, Si_3N_4, has received much attention in the last two decades, in the attempt to exploit the high-strength, heat-resistant properties of the fully-densified material. Current uses include cutting tool inserts, precision bearings, turbocharger rotors, and various diesel engine components, such as precombustion chambers and glow plugs. Details of silicon nitride formation can be obtained from several recent reviews [1–6].

One economically attractive method for the synthesis of Si_3N_4 ceramics is by the nitridation of silicon powder preforms to form a reaction-bonded body. This method results in a porous material with negligible shrinkage, which may be used directly, or post-densified to near theoretical values for high-performance applications (cf. [4]). The steps involved in the synthesis of reaction-bonded silicon nitride (RBSN) entail many features atypical of most gas–solid reaction systems, namely the retention of external dimensions of the compact while each of the individual silicon particles expands by 21.6 vol % (based on relative densities for 3 Si $\rightarrow$ Si_3N_4) and the sample increases in mass by 66.5% (based on molecular weights). Nitrogen diffusion into the macropores (i.e. the void space between individual silicon particles) and subsequent reaction results in the characteristic pore filling and density increase, and the reduction in pore size by two to three orders of magnitude [7]. Understanding of the fundamentals requires careful experimental practices in order to isolate the effects of one process parameter from another.

Many successful efforts in the past have elucidated the influence of several of these controlling factors, namely temperature [5, 6, 8], the sample heating profile [9, 10], particle shape and size distribution of the starting powder [8], impurities present in the sample (either native or added) [11–21], impurities derived from external sources such as the nitriding atmosphere and the furnace tube [21–23], composition of the nitriding atmosphere [24–37], pretreatment conditions [38], and whether the gas is static or flowing [39].

However, to our knowledge, there have been no published experimental reports in which intrinsic single-particle silicon nitridation kinetics were fully isolated from global or compact effects, and additionally, no differentiation has explicitly been noted between the two. As a result, past efforts have suggested that the nitridation process is characterized by a myriad of possibilities including linear [40–42], first-order for α-phase [43], second-order with iron present [20], logarithmic [30, 44], parabolic [42, 44, 45], phase-boundary controlled for β-phase [43], exponentially-decreasing [41], and mixed kinetics [8, 42, 43]. Mendelson's [46] general analysis of the earlier data suggests that the initial kinetics are reasonably well described by a close approximation to a linear rate law, which eventually succumbs to multi-stage rate laws. However, no generalizations could be made with regards to the rate-controlling mechanism in light of the wide variation of experimental conditions that were used to acquire the data, and the numerous complexities associated with the reaction-bonding process.

0022–2461 © 1993 Chapman & Hall

Hence, it is clear that a distinction must be made between intrinsic and global nitridation kinetics observed during the reaction-bonding process. Failure to do so renders the data tractable to a particular set of nitridation conditions, allowing for prediction in analogous systems, but fails to provide a priori prediction in a completely different system, and furthermore, reveals little detail about the actual nitridation mechanism. Additionally, it is important to realize that there may be a difference between the kinetics for the overall conversion of silicon to Si_3N_4, as opposed to the conversion to the individual phases, α and β. Their mechanisms of formation are quite different, and hence, as was first suggested by Jennings and Richman [42], one would expect at least two rate laws to be operative, which was recently also noted by Varma *et al.* [43]. In the majority of these global kinetic analyses, fitting with a particular model likely represents the combination of two or more intrinsic rate laws superimposed on each other, with the reaction conditions and extent of conversion determining which law is dominant at a given time. Hence, many have observed that one rate law appears to be operative at the early stages of nitridation, with a transition to a different rate law as the reaction proceeds. A first step in overcoming the obstacles of past analyses and elucidating intrinsic nitridation behaviour is through the use of near-spherical silicon powder with a narrow size distribution. Such powder would also be useful for manufacturing quality reaction-bonded products of high density through controlled packing and uniform surface area.

In view of these considerations, we have clarified and experimentally demonstrated some key aspects of the reaction-bonding process that have caused difficulties in past kinetic analyses. We have isolated intrinsic single-particle behaviour from global effects, and thus have established true silicon nitridation kinetics as a function of particle size (i.e. specific surface area) and temperature, yielding a rate law applicable to all systems. It is believed that an appreciation of the importance and an understanding of the intrinsic behaviour will be of benefit for future efforts in the design of appropriate experiments, and ultimately in the exploitation of reaction-bonded silicon nitride as a high-temperature structural ceramic.

2. Experimental procedure

The 99.999% silicon powder (− 325 mesh, < 43 μm, Cerac, Inc., Milwaukee, WI) used in these experiments was determined by spectrographic analysis to contain < 0.0001% Ca and 0.0002% Mg. Nitrogen adsorption indicated a BET area of 1.54 $m^2 g^{-1}$, while scanning electron microscopy (SEM), Fig. 1, clearly shows the wide range of particle sizes that result when silicon powder is prepared by ball-milling semiconductor-grade ingots. The crystals are faceted with sharp corners and range in size from about 43 μm to well below 1 μm. This is a typical method of preparing high-purity silicon powder, but unfortunately does not result in a powder with favourable characteristics for the production of high-quality, reaction-bonded silicon nitride components.

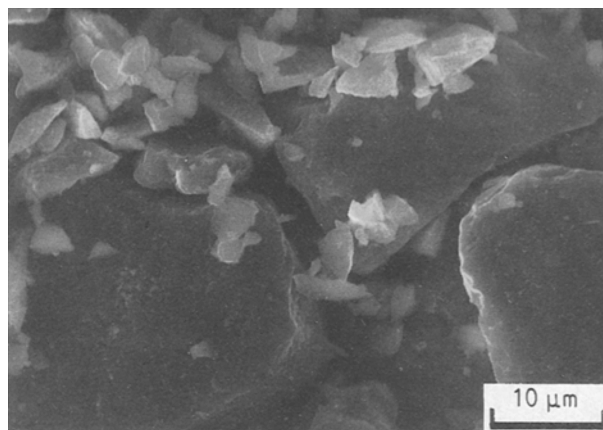

Figure 1 Scanning electron micrograph of the original silicon powder as obtained by ball-milling semiconductor grade ingots followed by mechanical sieving through a < 43 μm mesh.

Prior to its use, the silicon powder was jet-milled three consecutive times in an air-impact pulverizer (Trost Gem-T Research Model, Garlock Inc., New-town, PA) for reduction of average particle size, followed by mechanical sieving (GilSonic AutoSiever Model GA-6, Gilson Co., Inc., Worthington, OH) using electroformed nickel meshes to obtain four strictly-defined fractions of 5–10, 10–15, 15–20, and 20–37 μm. SEM verified the quality of the splits, Fig. 2, and showed that the jet-milling process removed most of the sharp angles and corners, resulting in more equiaxed and symmetrical crystals. X-ray diffraction (XRD) (nickel-filtered CuK_α) did not indicate the presence of any detectable SiO_2 that might have resulted from the milling and sieving processes. The BET areas of the powders were measured using nitrogen adsorption and are shown in Table I. Additional characterization was achieved using a Quantimet 570 (Cambridge Instruments Inc., Buffalo, NY) particle-size analyser. By digitizing SEM images of the various fractions, statistical data such as particle area, perimeter, shape factor, and equivalent diameter, were readily obtained. Each fraction was represented by several SEM images to ensure accurate and meaningful statistical data. A spherical-equivalent surface area was calculated for each of the four fractions, based on the average particle diameter determined by the Quantimet analysis. The resulting values were approximately 3–4.5 times smaller than those measured by nitrogen adsorption, and are an indication of the relative deviation from sphericity, and also suggest that the particle surfaces are not perfectly smooth, consistent with the SEM images shown in Fig. 2.

The nitridation kinetics were obtained using a Cahn 2000 recording electrobalance (1.5 g capacity; 0.5 μg sensitivity) equipped with a molybdenum-lined, high-purity alumina tube. Ultra-high purity gases were sent through a trap immediately preceding the furnace area, designed to reduce further the oxygen and water feed concentrations to < 50 p.p.b. (5×10^{-8} atm), and were accurately monitored using gas chromatography. In short, emphasis was placed on ensuring strict

TABLE I Particle size information for the silicon fractions obtained by jet milling and mechanical sieving of the − 325 mesh (< 43 μm) powder. The ultrafine particles (< 5 μm) were lost during the jet-milling process

Size fraction (μm)	Fractional breakdown by sieving (%)	BET area ($m^2 g^{-1}$)	Quantimet 570 average particle diam., (μm ± S.D.)	Calculated spherical equivalent area ($m^2 g^{-1}$) (based on Av. diam.)
37–43[a]	1.6	–	–	–
20–37	23.6	0.294	39.55 ± 1.30	0.065
15–20	30.0	0.453	18.99 ± 1.29	0.136
10–15	22.9	0.715	14.25 ± 1.34	0.181
5–10	21.9	1.108	7.30 ± 1.99	0.353

[a] Discarded.

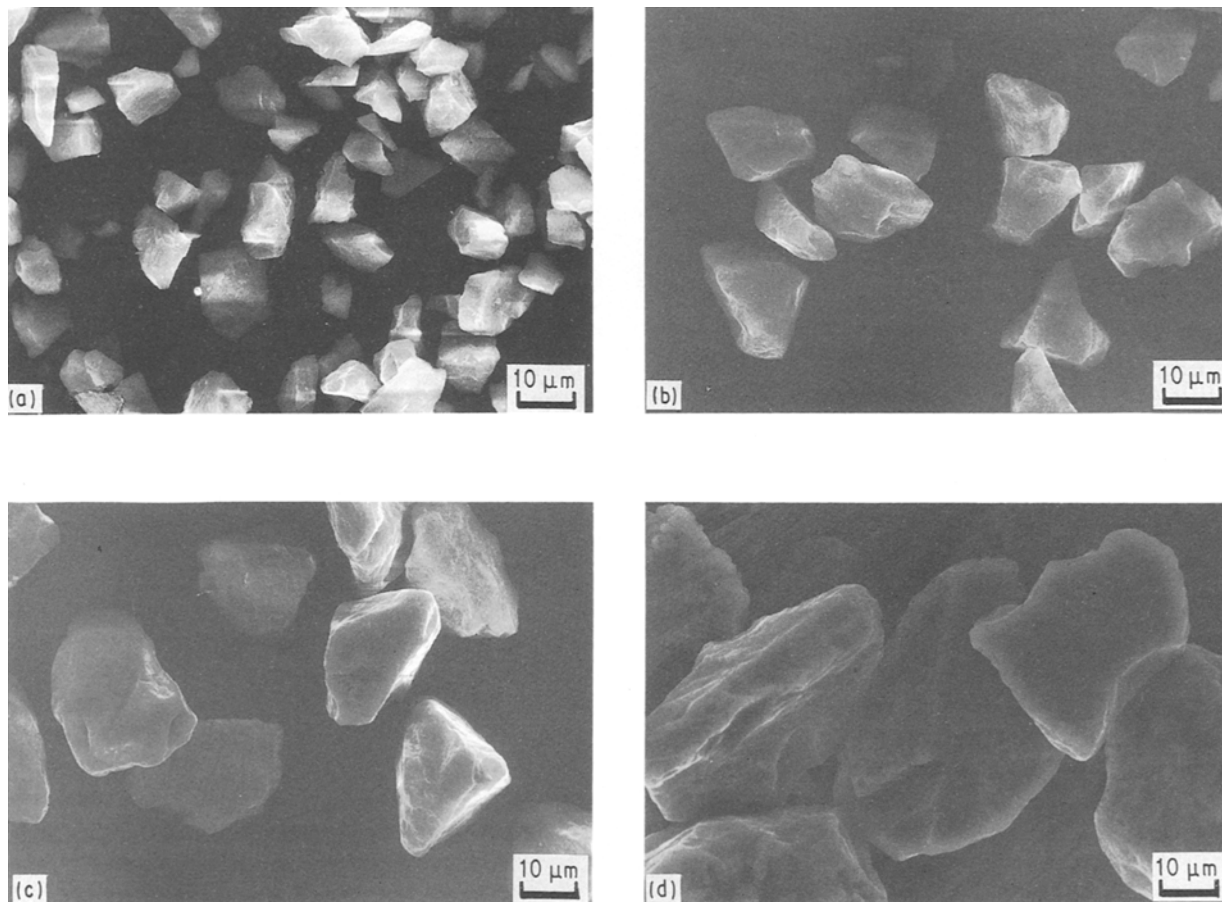

Figure 2 Scanning electron micrographs of the four fractions of silicon powder obtained by jet milling with subsequent mechanical sieving through precision electroformed nickel meshes. (a) 5–10 μm, (b) 10–15 μm, (c) 15–20 μm, (d) 20–37 μm.

control of the nitriding atmosphere, and avoiding potential sources of oxygen. Sample sizes varied between ~4 and 100 mg and were supported in 6 mm diameter molybdenum crucibles. For sample sizes greater than approximately 10 mg, an incipient volume of spectroscopic grade MeOH was added to the free powder resting in the crucible to yield a consistent packing density. Following extensive outgassing of the system, and allowing for the establishment of flow equilibrium, the furnace was heated at a maximum controller output from 20 °C (ambient) to 900 °C (a temperature too low for detectable nitridation) and then ramped in a linear profile to the desired soaking temperature (1175–1350 °C) at 340 °C h^{-1} (5.67 °C min^{-1}). Profiles for the heat-up to various temperatures are shown in Fig. 3. This was done to allow for reproducibility of the thermal profile. Time zero for the nitridation experiments was taken as the point at which the furnace heat-up was initiated. Data acquired by the TGA system was resolvable to 0.01 mg. Additional details of the apparatus and the experimental procedure are described elsewhere [21].

Owing to small sample sizes used for the intrinsic kinetic data (4.6 mg), emphasis was placed on making sure that the mass changes were attributed to the proper source. Factors considered included (1) the volatility of the silicon at reaction temperatures, (2) weight variations in components of the TGA system, and (3) momentum effects on the crucible due to increase in the linear flow rate as the gases undergo

thermal expansion when heated from ambient to reaction temperature as they pass through the furnace.

This first aspect was addressed by conducting silicon volatilization studies to determine the magnitude of the losses at elevated temperatures. These results are reported in Section 3.1, and indicate the magnitude of the correction deemed appropriate, for the mass of silicon present at any given time during the nitridation process. This is a modest correction, but lends greater credibility to the interpretation of the kinetic data. Weight variation in the TGA components was addressed by pre- and post-weighing all parts of the system that might undergo mass changes either by deposition (gain) or by volatility (loss). These components included the molybdenum crucible, the Si/Si_3N_4 reacted sample, and the tungsten wire support used to attach the molybdenum crucible to the sapphire hangdown fibre. The final aspect (momentum effects) was addressed by studying the weight changes indicated by the TGA on an empty molybdenum crucible heated with the standard furnace profile to 1350 °C, and held at that temperature for over 20 h. This yielded the weight variation profile during heat-up (e.g. 0–0.45 mg total gain at 1350 °C following a linear profile) which provided the necessary correction, and also demonstrated that no significant volatility of the molybdenum crucible (possibly as MoO_3) occurred under the stated nitridation conditions.

Post analysis of the samples was accomplished using optical microscopy and an SEM equipped with an energy dispersive X-ray analyser. XRD was used for quantitative phase determination in samples of sufficient size ($\geq$ 25–30 mg) which permitted accurate powder diffraction profiles to be obtained [47].

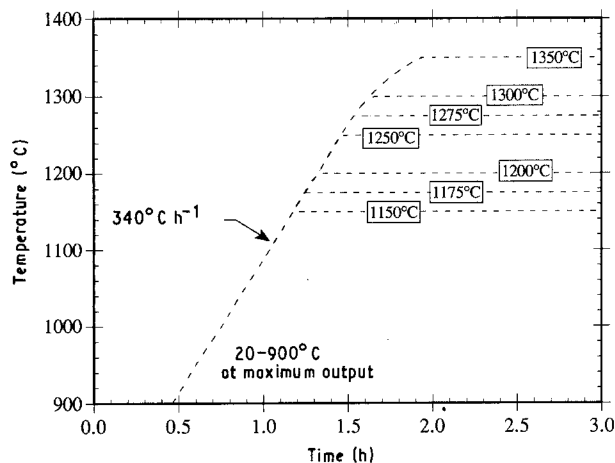

Figure 3 Temperature–time profiles for furnace heat-up to various soaking temperatures.

3. Results and discussion

3.1. Silicon vaporization studies

The volatility (loss) of silicon at reaction temperatures was determined by using 38.3 mg of the 5–10 μm silicon fraction sample. The sample was heated in a 5% H_2–95% He mixture following the standard furnace profile to ultimate holding temperatures of 1250, 1300, 1350 and 1400 °C. The total gas flow rate was $150\ cm^3\ min^{-1}$. At each temperature, the sample was allowed to soak for 4 h to determine the corresponding loss, expressed in units of $kg\ m^2\ s^{-1}$, i.e., 1 kg silicon vaporizing per second per unit total surface area exposed to the nitriding atmosphere.

The area available for evaporation was determined by dividing the total surface area of the powder (using BET area = $1.11\ m^2\ g^{-1}$) by the number of layers of silicon particles expected to reside in the 6 mm diameter crucible, and then dividing by a factor of two. This yields a modified area for the exposed silicon particles that takes into account the undulations of the top surface of the powder resting in the crucible. An obvious error would result if the evaporation area was taken simply as the geometric top surface of a 6 mm diameter cylinder, thus yielding too small a value. This modified area also recognizes that particles within the compact are not likely to contribute significantly to the observed evaporation rate, because any silicon that does vaporize in the macropores will likely recondense as it strikes a nearby surface. The evaporation rates obtained are summarized in Table II and are compared with the theoretical values calculated using Langmuir's equation [48], which is based on the kinetic theory of gases and establishes a relationship between vapour pressure and rate of evaporation. The actual mass loss for the given sample size varied from $0.231\ mg\ h^{-1}$ at 1250 °C up to $0.902\ mg\ h^{-1}$ at 1400 °C. This aspect of silicon vaporization was taken into account in the interpretation of the nitridation data.

An interesting point is that these observed vaporization rates are slightly larger than the maximum nitridation rate (i.e. the maximum per cent weight change in unit time) ever observed during the reaction-bonding process. In experiments at 1350 °C using the 5–10 μm silicon, the highest nitridation rate observed was $1.1 \times 10^{-7}\ kg\ m^{-2}\ s^{-1}$, which translated to 65.24% conversion per hour, compared to an observed evaporation rate of $9.7 \times 10^{-7}\ kg\ m^{-2}\ s^{-1}$ for the free silicon powder. This suggests that the vaporization of silicon and its subsequent reaction with nitrogen in the gas phase is more than adequate to sustain the observed nitridation rates, as was also

TABLE II Silicon evaporation rates obtained between 1250 and 1400 °C at $150\ cm^3\ min^{-1}$ total flow rate

Temp. (°C)	Sample mass (mg)	Total surface area (m^2)	No. of layers	Modified area ($10^{-4}\ m^2$)	Evaporation rate ($10^{-7}\ kg\ m^{-2}\ s^{-1}$)	Langmuir rate ($10^{-6}\ kg\ m^{-2}\ s^{-1}$)	Relative diff. in magnitude
1250	38.30	0.042 130	144	2.925	4.39	0.795	1.8
1300	36.62	0.040 282	139	2.898	6.19	2.88	4.6
1350	35.52	0.039 072	135	2.894	9.72	7.70	7.9
1400	33.76	0.037 136	128	2.901	17.3	19.0	11

noted by Moulson [6] in his attempt to justify the feasibility of $Si_{(g)}$ nitridation as one of the reaction pathways to produce $Si_3N_{4(s)}$.

3.2. Effect of compact size

The influence of compact formation on the nitridation kinetics was elucidated by following the rate and extent of conversion for the nitridation of the 5–10 μm silicon fraction at 1350 °C in a 5% H_2/N_2 mixture. The narrow particle-size distribution minimizes effects normally attributable to packing variations in the green compact, while the constant diameter (6 mm) molybdenum crucible allows the compact size to be varied in a single dimension by simply adjusting the amount of silicon placed in the holder between 4.6 and 102 mg. The 4.6 mg sample represents the maximum rate and shortest time to full conversion that can ever be observed with the 5–10 μm fraction under the stated nitridation conditions, and hence, represents true intrinsic behaviour.

Fig. 4 illustrates the effect of the compact size and shows that a greater fraction of silicon is converted to silicon nitride in a given period of time for the smallest compact. Additionally, the smaller sample sizes maintain the initial (maximum) rate up to a higher level of conversion. This variation in nitridation behaviour is due to sealing-off of the inner silicon particles from availability of nitrogen as reaction proceeds, and is evidenced by the "kneeing" in the conversion versus time behaviour. The effects are also readily observable in a cross-section of the compact by the formation of a "watermelon-like" skin on the outer edges. It is possible that large sample sizes may never reach full conversion unless the nitridation environment is significantly altered, e.g. by increasing the temperature above the melting point of silicon (1413 °C) or increasing the partial pressure of nitrogen. Even then, success at reaching full conversion may be marginal. Additional considerations resulting from compact effects have recently been noted [21].

A very interesting feature of the observed kinetic behaviour is that the initial rate appears to be unaffected by the sample size (thickness), suggesting that in the early stages, up to about 20%–25% conversion, there is uninhibited diffusion of nitrogen into all regions of the compact. So regardless of whether the particles are near the centre of the compact or near the outer edge, they are exposed to identical bulk nitrogen concentration. Indeed, a simple calculation indicates that the maximum per cent conversion achievable based on all the macropores (0.5 void fraction) being filled with nitrogen at time zero, with no further influx of additional nitrogen, would only be on the order of 0.014%. Thus, there is no limitation arising from diffusion of nitrogen during the early stages of nitridation, and therefore, during this period the particles nitride at their maximum intrinsic rate.

The observed nitridation behaviour is summarized qualitatively in Fig. 5 and can be described in the following manner. In the initial stages of nitridation, stage 1, nitrogen diffuses freely throughout all regions of the compact, its macroscopic concentration remains essentially constant, and hence all particles are exposed to identical conditions and react in an analogous manner following the same intrinsic rate up to about 20%–25% conversion depending on the mass (thickness) of the sample. With further progression of the reaction, stage 2, there is a corresponding increase in the volume of the individual grains resulting in a decrease of permeability in the macropores. This increase in volume is especially evident for particles near the outer edges of the compact (including those adjacent to the molybdenum crucible due to higher

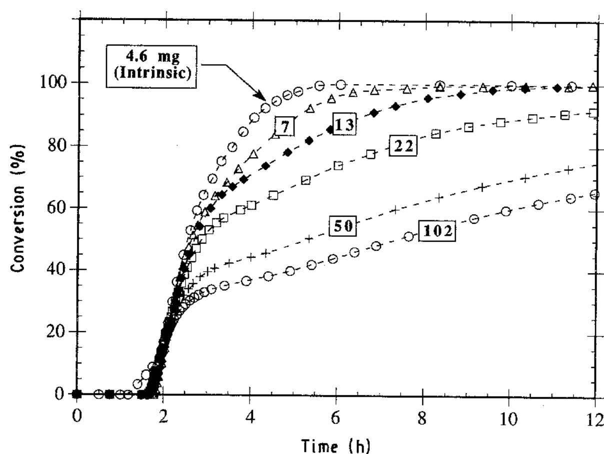

Figure 4 Effect of compact size on the nitridation of 5–10 μm silicon powder ranging from 4.6 mg (intrinsic behaviour) to 102 mg. (1350 °C, 5% H_2/N_3, 150 cm^3 min^{-1}.)

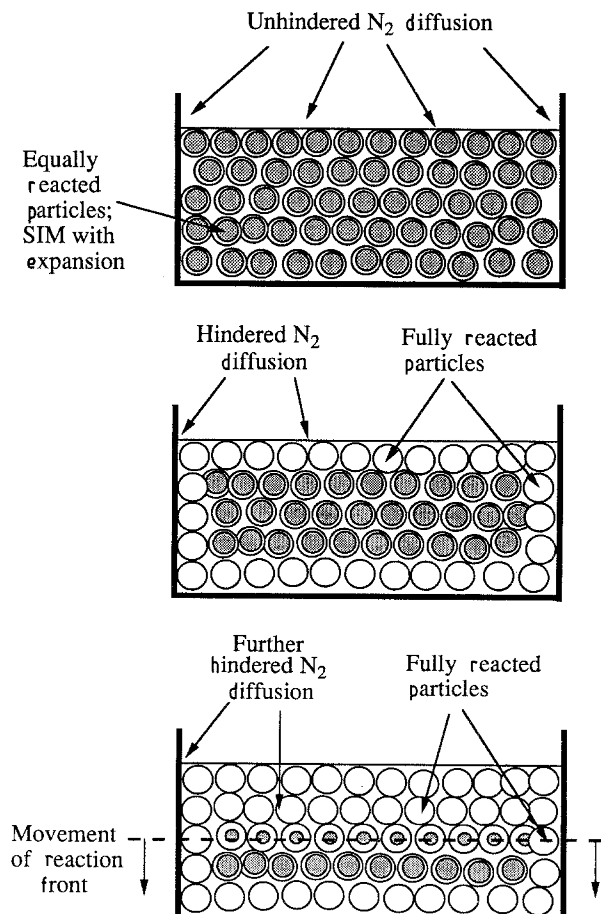

Figure 5 The various stages observed during the nitridation of silicon powder supported in a molybdenum crucible.

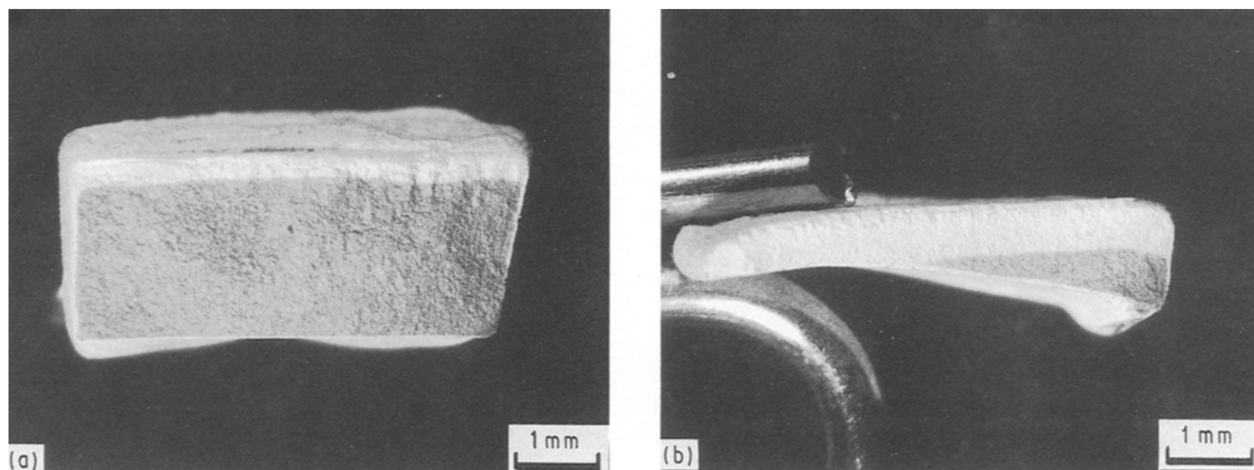

Figure 6 Optical micrographs of the fracture surfaces of partially reacted silicon compacts showing "watermelon-skin" formation encompassing the sample, and the linear propagation of the reaction front due to the presence of the molybdenum crucible: (a) 100 mg sample at 66% conversion, (b) 20 mg sample at 92% conversion.

void fraction near the walls initially), because these particles are the first to be exposed to the flowing nitrogen. With particle expansion, nitrogen diffusion becomes restricted, a white Si_3N_4 layer encloses the compact, and the characteristic "kneeing" in the conversion versus time curve is observed. Thus in stage 3, the only remaining pathway for nitrogen to reach the partially reacted particles in the centre of the compact is for it to diffuse through the top layer. This results in a one-dimensional propagation of the reaction front towards the bottom of the compact. Direct evidence of this behaviour is shown in the optical micrographs in Fig. 6.

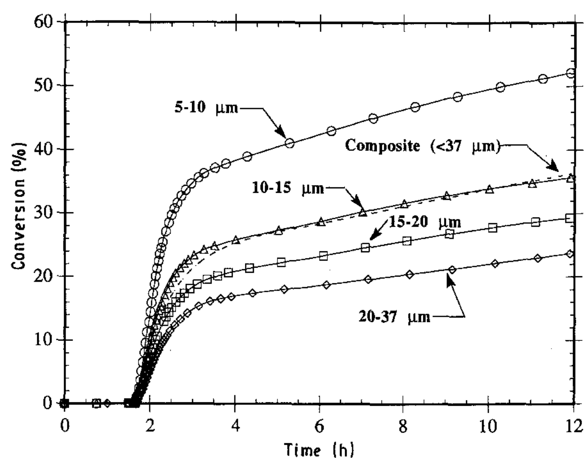

Figure 7 Effect of particle size on the nitridation behaviour. (---) The unsieved powder (composite, < 37μm) is shown for comparison. (100 mg, 1350 °C, 5% H_2/N_2, 150 cm^3 min^{-1}.)

3.3. Effect of particle size

The influence of particle size was studied by nitriding similar quantities ($\approx$100 mg) of the various silicon fractions at 1350 °C in a 5% H_2/N_2 mixture. The results are shown in Fig. 7. As expected, the smaller particles react with a greater initial rate (as determined by the maximum slope observed) and reach a higher conversion in a given amount of time. This can be attributed to the increase in the reactive surface area per unit mass, thereby enhancing the exposure between the silicon and nitrogen, and by increasing the area available for silicon vaporization. For comparison, the nitridation kinetics of the composite powder (< 37 μm) is also shown, its behaviour being very similar to the 10–15 μm fraction. An important observation is that the maximum initial rate varies with the particle size, suggesting that the intrinsic single-particle behaviour is a function of the specific surface area. This aspect is accounted for in the development of the intrinsic rate equation in Section 3.5.

Because these nitridation curves represent the behaviour of "compacted" powder, one might expect an optimum particle size to exist so that maximum rates and highest conversion are achieved. Large particles provide large macropores, but at the expense of decreased surface area. On the other hand, small particles provide increased reactive surface area for the same void fraction, but lead to smaller macropores which inhibit nitrogen diffusion. In both cases, less than optimum kinetics would result. However, this latter aspect was not observed in these experiments, suggesting that even for particles as small as 5 μm, the macropores are still sufficiently large. This may not carry over to the nitridation of ultrafine silicon powder (50–200 nm), due to global (compact) effects overwhelming the expected enhancement associated with the large increase in surface area (e.g. [49]).

In preliminary experiments to elucidate the intrinsic kinetics of ultra-fine silicon (70–90 nm) prepared via silane pyrolysis, it was evident that agglomeration (500 μm typical), even in the "free" powder, was sufficient to impart strong compact effects. Thus the likelihood of ever exploiting ultrafine silicon for the manufacture of RBSN bodies is questionable. A more practical route would employ direct nitridation during powder synthesis to produce ultrafine $Si_3N_{4(s)}$ instead (cf. [50–52]), followed by hot isostatic pressing or alternative densifying methods.

3.4. Intrinsic nitridation kinetics

In order to establish intrinsic kinetics, minimal sample sizes need to be employed. Ideally, the nitridation experiments would be conducted using a single particle of silicon of a given size (e.g. 10 μm), suspending it in the TGA system, and observing the nitridation behaviour. Experimentally, such an exercise is not feasible, owing to the extremely small weight variations that would be observed as the sample reacted, and hence, would be overwhelmed by noise resulting from static and other limiting factors noted in Section 2. In short, the weight increase would be beyond the resolution of the TGA system.

An alternative approach entails the use of many particles, so that weight increases are significant, but not too many such that compact effects are observed. This is achieved experimentally by placing a very thin layer of silicon particles on the bottom of the molybdenum crucible in a manner such that the particles nitride independently of each other. Hence, compact effects are minimized and the intrinsic behaviour is elucidated. Preliminary experiments were carried out to determine the optimum sample size. No changes in the conversion versus time behaviour were observed for samples ≤ 4.6 mg, and hence this mass was chosen to maximize weight gain and minimize noise.

Fig. 8 shows the intrinsic kinetic behaviour resulting from the influence of particle size. As expected, the smaller particles reacted at a greater rate and reached a higher conversion in a given amount of time for reasons noted in Section 3.3. An important feature brought to light is that, because the initial rate (i.e. the maximum rate in moles of silicon reacted per unit time) varies with particle surface area, the intrinsic kinetics cannot be adequately described by a homogeneous rate law such as $dx/dt = k(1 - x)^n$, where x is the conversion of silicon, k is the reaction rate constant, and n is the reaction order for the fraction of unreacted silicon $(1 - x)$. Therefore, any modelling of the nitridation process (intrinsic and reaction-bonding) requires structural characteristics to be included in the description.

Another interesting point shown in Fig. 8 is that particles as large as 37 μm reached full conversion.

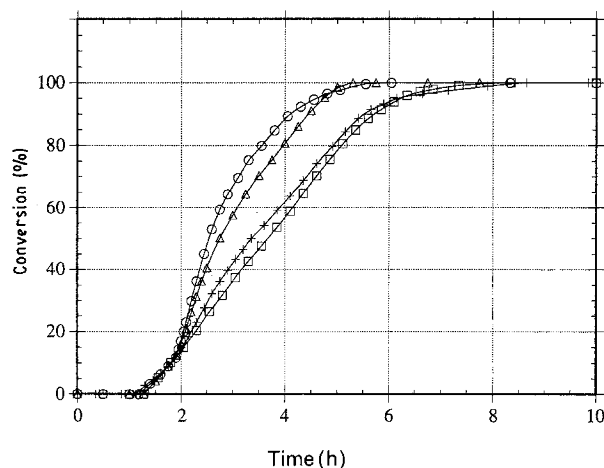

Figure 8 Intrinsic nitridation behaviour as a function of particle size at 1350 °C. (4.6 mg, 5% H_2/N_2, 150 $cm^3\ min^{-1}$.) (○) 5–10 μm, (△) 10–15 μm, (+) 15–20 μm, (□) 20–37 μm.

This is somewhat surprising considering previous work which noted that particles on the order of ≤ 5 μm may be required to attain full conversion in a reasonable amount of time [2]. Atkinson *et al.* [53], however, estimate that pure silicon particles up to 30 μm diameter may be nitrided to full conversion using sub-atmospheric nitrogen pressures (≈0.067 bar) based on their observations of 75% conversion in 75–100 μm particles.

It is clear that in order to nitride fully a 37 μm particle, the Si_3N_4 product layer must maintain reasonable microscopic porosity, albeit small (≪ 1 μm), throughout the course of the reaction. This can be in the form of micropores in the α-matte and whiskers, and as channels in the *c*-axis of the β-crystals ($D_\beta = 7.2 \times 10^{-19}\ cm^2\ s^{-1}$; 1350 °C [54]). Nitridation may also result from nitrogen diffusion through single-crystal α-Si_3N_4 ($D_\alpha = 3.8 \times 10^{-20}\ cm^2\ s^{-1}$; 1350 °C [54]) that forms as the product layer densifies. The latter two pathways are expected to contribute at a much lower rate, however. Regardless of the pathway for nitrogen delivery, the nitridation of a single particle of $Si_{(s)}$ to $Si_3N_{4(s)}$ appears to follow a sharp-interface model (SIM) (e.g. [55, 56]), modified to take into account the expansion in volume as the particle reacts. We can envision a Si_3N_4 product layer developing on the silicon particle, through which reacting gases diffuse to reach the unreacted core. A sharp interface may result under two conditions: (1) when the reaction at the Si–Si_3N_4 interface is rapid relative to the rate of nitrogen diffusion through the product layer, or (2) when the unreacted inner core is essentially non-porous, as is the case for silicon. In the latter situation, the relative rates of diffusion and reaction determine the rate-limiting step in the SIM model.

The linear conversion versus time behaviour observed at the early stages of nitridation appeared to be independent of the silicon particle size (zero-order), Fig. 8. Additionally, it was found to be sensibly independent of the furnace temperature between 1100 and 1350 °C and of the extent of conversion. This behaviour can be attributed to either (1) devitrification of the SiO_2 layer or (2) initial nucleation following the model proposed by Atkinson *et al.* [41]. The integrity of the inherent SiO_2 layer (≈3 nm thick) may be such that it does not permit silicon to readily volatilize, and prevents nucleation via nitrogen adsorption, masking the true intrinsic rate until it is sufficiently fractured. This is one possible explanation. The nucleation process itself would not be expected to be completely independent of temperature. Increasing the temperature should decrease adsorption, and therefore decrease nucleation. Counter-effects would include the enhancement in silicon volatility, diffusion coefficients, and the Arrhenius rate constant, which would all increase the observed rate. A cancelling of these effects, i.e. nucleation relative to volatility, diffusion, and reaction, to yield the zero-order region is an unlikely scenario.

Fig. 9 shows the intrinsic kinetic behaviour resulting from the influence of reaction temperature. 5–10 μm silicon was nitrided in a 5% H_2/N_2 mixture at temperatures ranging between 1200 and 1350 °C. As

expected, faster rates and greater overall conversion are observed with increasing temperature, suggesting that the intrinsic rate is also a function of T. As in the previous intrinsic data reflecting particle-size effects, the maximum rate was achieved after the final soaking temperature had been reached, so in all cases isothermal rates were observed.

Based on the maximum slopes from both sets of intrinsic kinetic data, it was possible to determine what we herein refer to as the initial intrinsic rate, R_i, with Fig. 8 at constant T–variable S_a, and Fig. 9 at constant S_a–variable T. This information was then used to develop an intrinsic kinetic expression appropriate for all nitriding systems, and to elucidate additional features of the nitriding mechanism.

3.5. Intrinsic rate equation

Noting the dependence of the intrinsic data with surface area and temperature, and acknowledging the current understanding of the mechanisms of α- and β-phase formation, an appropriate representation for the intrinsic rate (moles silicon reacted/time) is given as

$$R_i = (S_a)^{\gamma} k(T) (C_{N_2})^{\delta} \quad (1)$$

where S_a is the specific surface area of the silicon powder ($m^2\,g^{-1}$), C_{N_2} is the bulk concentration of nitrogen, $k(T) = k_0 \exp(-E_a/RT)$ is the Arrhenius rate constant, and γ and δ are the reaction orders for surface area and nitrogen concentration, respectively. For the initial (or maximum) rate, S_a is the specific surface area indicated in Table I. In excess nitrogen, Equation 1 can be rewritten to reflect the independence of nitrogen concentration

$$R_i = (S_a)^{\gamma} k'(T) \quad (2)$$

where

$$k'(T) = k(T)(C_{N_2})^{\delta} = k'_0 \exp\left(-\frac{E_a}{RT}\right) \quad (3)$$

and $k'_0 = k_0(C_{N_2})^{\delta}$. The idea of "excess" nitrogen can be understood as follows. At atmospheric pressure, the maximum rate of mass increase by a 4.6 mg (intrinsic) sample reacting at 1350 °C is approximately 2.0 mg h^{-1} (specifically 65.24% conversion per hour) which translates to 0.03 cm^3 min^{-1} N_2 at STP actually reacting. Obviously, at a flow rate of 150 cm^3 min^{-1}, excess nitrogen is present that does not react but may be intimately involved in other aspects of the reaction, such as the transport of impurities to and from the reaction site, altering various transport properties of the nitriding gas [35–37], and by removing silicon vapour, thereby lowering p_{Si} and encouraging further vaporization. This latter aspect has been shown to encourage pore formation and coarse product, resulting in reduced mechanical strength [28, 39]. In our context, "excess" nitrogen refers simply to a surplus of nitrogen required to sustain the observed maximum rate of reaction.

Equation 2 can be linearized as

$$\ln R_i = \gamma \ln(S_a) + \ln k'_0 - \left(\frac{E_a}{R}\right)\frac{1}{T} \quad (4)$$

By varying the surface area (particle size) and maintaining constant temperature, we can establish γ from the slope and k'_0 from the intercept of the plot of ln R_i versus ln (S_a). Likewise, E_a can be established by maintaining constant surface area and varying the temperature, and by making an analogous plot of ln R_i versus $(1/T)$. Using the intrinsic data shown in Figs 8 and 9 for the effects due to surface area and temperature, respectively, we can obtain R_i for the various conditions by drawing a tangent to the conversion versus time curve at the point where the maximum rate is observed. As was noted previously, this rate always occurs under isothermal conditions, i.e. after the furnace has reached its final soaking temperature. Table III summarizes these values.

Least squares analysis for the plot of ln R_i versus ln S_a yielded a correlation coefficient of 1.00, and similarly, for the plot of ln R_i versus $(1/T)$ a coefficient of 0.999. The corresponding values for the kinetic parameters, γ, k'_0 and E_a were determined to be 0.843, 5.0×10^7, and 301.5 kJ mol^{-1}, respectively. These parameters, together with Equation 2, fully define the intrinsic rate as function of surface area and temperature under conditions of excess nitrogen

$$R_i = -\frac{dS_i}{dt} = 5.0 \times 10^7 \exp\left(-\frac{301.5\ \text{kJ mol}^{-1}}{RT}\right) \times (S_a)^{0.843}\ (\text{moles Si reacted h}^{-1}) \quad (5)$$

Because the intrinsic data were obtained using the same quantity of silicon (i.e. 4.6 mg) for all the runs, and based on our definition of the initial single-particle intrinsic rate

$$R_i = (R)_{t=t_{max}} = \text{Si}(0)\left(\frac{dx}{dt}\right)_{t=t_{max}} \quad (6)$$

TABLE III Intrinsic rates obtained under various nitridation conditions

Run	Temp. (°C)	BET area ($m^2\,g^{-1}$)	R'_i, (% conv. h^{-1})	R_i, (10^3 mol h^{-1})
1	1350	0.294	21.32	3.477
2	1350	0.453	31.20	5.110
3	1350	0.715	45.79	7.500
4	1350	1.108	65.24	10.685
5	1300	1.108	33.84	5.542
6	1275	1.108	22.36	3.662
7	1250	1.108	15.10	2.473

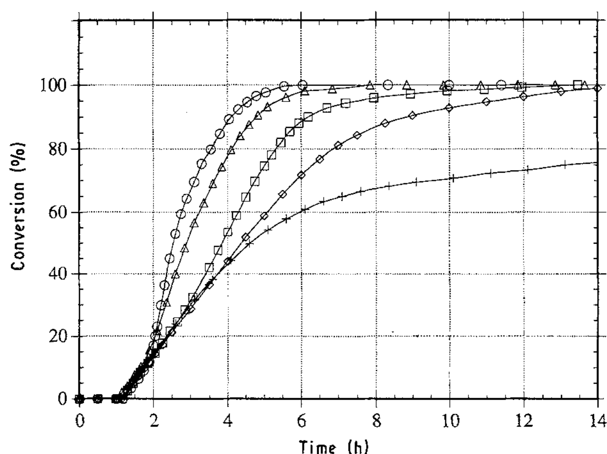

Figure 9 Intrinsic nitridation behaviour as a function of temperature for 5–10 μm silicon. (4.6 mg, 5% H_2/N_2, 150 $cm^3 min^{-1}$.) (○) 1350 °C, (△) 1300 °C, (□) 1275 °C, (◇) 1250 °C, (+) 1200 °C.

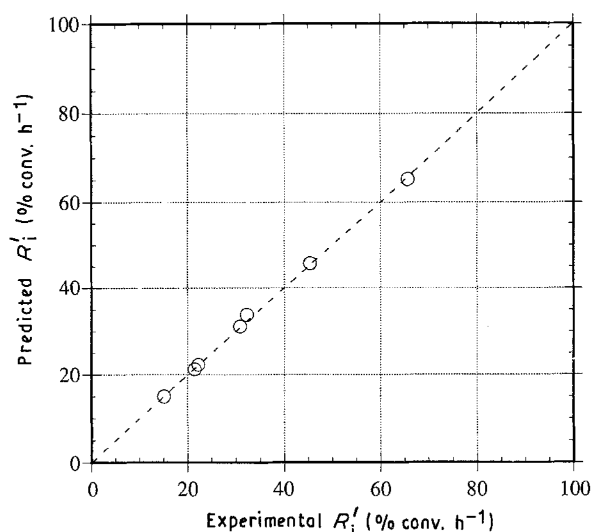

Figure 10 Plot of the predicted maximum intrinsic rates versus the rates observed experimentally. Excellent correlation was achieved.

where $t = t_{max}$ represents the time at which the maximum rate is observed, Equation 5 can alternatively be written in terms of % conv. h^{-1} by dividing by the number of moles of silicon present at $t = 0$

$$R_i' = \left(\frac{dx}{dt}\right)_{t=t_{max}} = 3.052 \times 10^{11} \exp\left(-\frac{301.5 \text{ kJ mol}^{-1}}{RT}\right)(S_a)^{0.843} (\% \text{ conv. h}^{-1}) \quad (7)$$

As a final check, Fig. 10 shows the comparison between the predicted rates calculated from Equation 7 and those obtained experimentally, and demonstrates good correlation between the two as indicated by their relative position to the 45° line.

The 0.843 reaction order for the dependence on solid surface area is close to a first-order dependence on surface area typically assumed for gas–solid reactions [55–57]. This is expected because the initial rate should be proportional to the available surface area for nucleation and silicon vaporization, and furthermore, should be independent of the actual geometry of the silicon particles, i.e. any deviation from true sphericity. The departure from unity may be attributed to three main factors: (1) the partial pre-sintering that occurs prior to nitridation as the silicon particles are heated from 20 °C to their final soaking temperature could decrease the available surface area (i.e. relative to that measured at 77 K), thereby yielding observed rates slightly lower than what would be expected, most notably for the smaller particle sizes; (2) the fact that the maximum rates are obtained subsequent to the linear region at the initial stages of nitridation, implies that some reaction has already occurred (~20% conversion, Fig. 8), and therefore there could be marginal particle interactions even with the small sample size; and (3) the inherent complexities involved in silicon nitridation that do not allow the process to be described so simply.

An activation energy of 301.5 kJ mol^{-1} suggests that the process is diffusion-controlled through the Si_3N_4 product layer developing on the individual grains. It is interesting to note that this experimentally obtained activation energy for the overall conversion of silicon to Si_3N_4 lies between those reported for the diffusion of nitrogen in polycrystalline α-Si_3N_4 (233 kJ mol^{-1}) and β-Si_3N_4 (777 kJ mol^{-1}) [54], and furthermore, its value is closer to that of the α-phase, which is consistent with the high α/β phase ratio typically obtained in the nitridation of high-purity silicon below its melting point (1413 °C). This would suggest that the product layer developing on the individual grains is predominantly α-phase, which was verified by XRD and SEM analyses, but more importantly, that this layer is of fairly high integrity with minimal porosity.

3.6. SIM kinetic analysis

Based on the intrinsic nitridation behaviour, where fairly equiaxed particles as large as 37 μm were shown to nitride to full conversion, and where the process was shown to be dependent on surface area and highly sensitive to temperature ($E_a = 301.5$ kJ mol^{-1}), suggests that the conversion of a single particle of silicon to Si_3N_4 could be well described by a sharp-interface model (SIM) with product layer expansion under conditions of diffusional control. Indeed, the silicon particles themselves are non-porous, so reaction occurs in a relatively thin zone demarcating the Si–Si_3N_4 interface. A schematic representation of the sharp-interface model is shown in Fig. 11.

Microstructural evidence in the nitridation of single-crystal silicon [41, 58–61] is clearly supportive of this view. A cross-section of a single crystal of silicon is shown in Fig. 12, illustrating the formation of the Si_3N_4 product layer (generally high α/β) developing at a sharp interface with the non-porous silicon. With continued reaction, the interface recedes towards the centre of the grain. One typically observes (1) α-matte (nuclei) formation, Fig. 13a, as described by the nitrogen–chemisorption model developed by Atkinson *et al.* [41], along with (2) fine α-whisker growth (0.05–0.2 μm diameter) on the surface of the silicon, Fig. 13b, and into the pores, Fig. 13c.

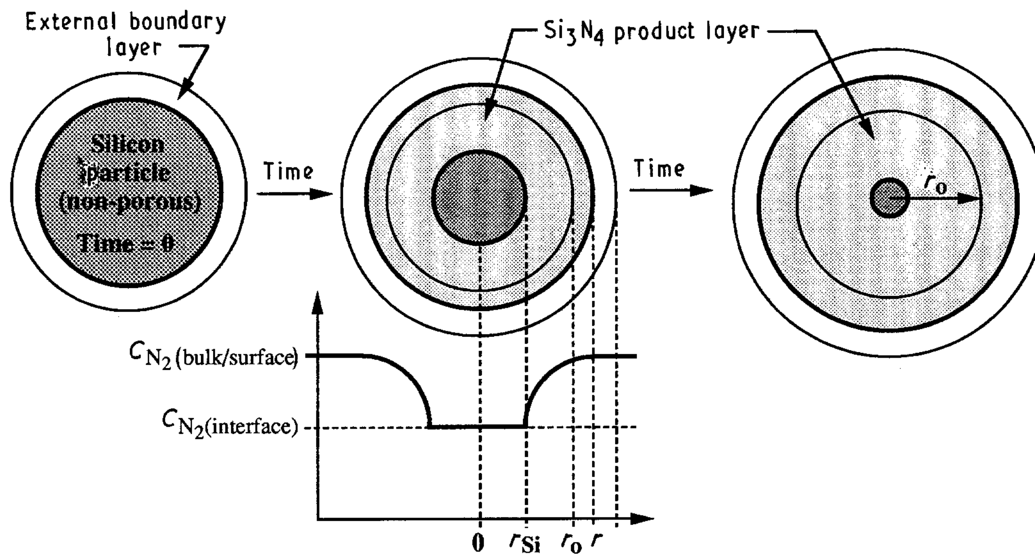

Figure 11 Schematic representation of a silicon particle reacting as an expanding sharp-interface model, under diffusion control through the developing Si_3N_4 product layer. r_0 = initial particle radius, r = particle radius at time t, r_{Si} = radius of unreacted silicon core at time t.

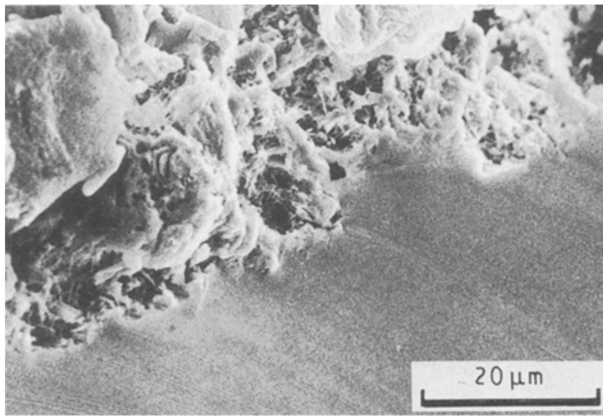

Figure 12 Cross-section of single-crystal silicon partially nitrided at 1350 °C in 5% H_2/N_2 illustrating the relatively sharp interface between the non-porous silicon and the developing Si_3N_4 product layer (predominantly of α-phase).

α-whisker formation is believed to occur through a vapour–liquid–solid (VLS) mechanism [42], or simply through a chemical vapour deposition (CVD) process between $Si_{(g)}$ and $N_{2(g)}$. This latter mechanism is probably the dominant mode of formation under flowing nitrogen. The presence of impurities may enhance the formation of α-whiskers by liquid formation at the base or at the terminus (via a VLS mechanism), but does not appear to be necessary. This has been substantiated by α-whisker development in pores deep within the silicon grain where impurities are unlikely, and also by our observations of high α/β phase ratios typically obtained with ultrapure silicon nitrided below melting temperatures [21]. To a lesser extent, β-phase will also accompany the growth of the nitride layer, Fig. 13d, forming through a gas–solid reaction with the silicon surface, through diffusion of atomic nitrogen along the *c*-axis of the β-crystal [42], or in the presence of liquid phase which may stimulate its production [14, 21].

In the SIM model, three rates are of interest: (1) the diffusion of nitrogen through the gas film surrounding the particle, i.e. external mass transfer, (2) the diffusion of nitrogen through the developing Si_3N_4 product layer, and (3) the chemical reaction at the Si–Si_3N_4 interface. The limiting rate will determine the reaction kinetics, unless, of course, two or more rates are of the same order of magnitude.

Under conditions of diffusion control through the Si_3N_4 product layer, in the presence of product layer expansion, this model reduces to [56]

$$\frac{1}{(Z-1)}\{Z - [(1-Z)(1-x) + Z]^{2/3}\} - (1-x)^{2/3} = \left(\frac{2\eta C_{N_2} M_w D_{eff}}{\rho_{Si} r_0^2}\right) t \quad (8)$$

where r_0 is the original radius of the silicon particle, D_{eff}, the effective diffusivity for nitrogen diffusion through the Si_3N_4 product layer; η the stoichiometric coefficient $Si/N_2 = 3/2$; C_{N_2} the surface (or bulk) concentration of nitrogen ($g_{mol} \cdot cm^{-3}$), M_w, the molar mass of silicon, ρ_{Si}, the density of silicon, x the fractional conversion, and t time. The quantity Z is defined as

$$Z = \frac{\text{volume of product } Si_3N_4 \text{ formed}}{\text{unit volume of Si reacted}} = \left(\frac{M_w}{\rho}\right)_{Si_3N_4}\left(\frac{\rho}{M_w}\right)_{Si}\left(\frac{\eta_{Si_3N_4}}{\eta_{Si}}\right) = 1.216 \quad (9)$$

Equation 8 yields a linear relationship for the left-hand side versus time, assuming a sensibly constant value for D_{eff}, with the slope given as the quantity in parenthesis. The physical meaning of this equation is that it gives the time required to achieve a given conversion, x, for an expanding grain of silicon as it forms Si_3N_4, if the process were controlled entirely by diffusion through the product layer, i.e. the relative rates of diffusion through the external boundary layer and chemical reaction at the interface are much faster. With this at hand, linear plots were drawn using the intrinsic data shown in Fig. 9, evaluating r_0 using a normalized length scale, L, typical of intraphase

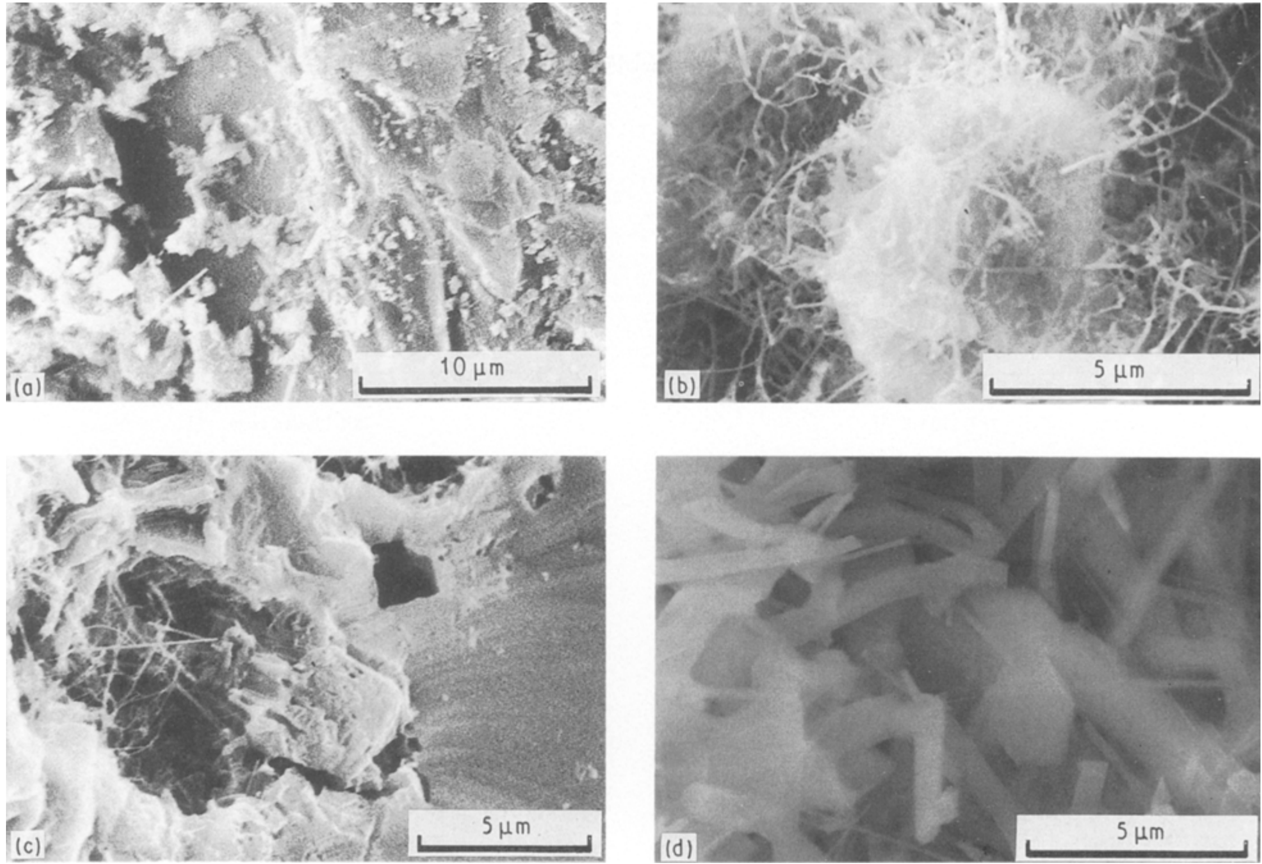

Figure 13 Microstructural development observed during nitridation. (a) Formation of α-Si_3N_4 nuclei on an irregular silicon surface (1350 °C, 5% H_2/N_2); (b) α-Si_3N_4 whisker growth on the surface of a 5–10 μm Si particle during the initial stages of nitridation (< 10% conversion) (1175 °C, 5% H_2/N_2, 150 $cm^3 min^{-1}$); (c) α-Si_3N_4 whisker growth within a pore at the Si–Si_3N_4 interface (1350 °C, 5% H_2/N_2, 150 $cm^3 min^{-1}$); (d) interlocking, hexagonal β-Si_3N_4 growth accompanying the development of the fine α-whiskers within the Si_3N_4 product layer.

diffusion-reaction problems [62]

$$L = \frac{\text{particle volume}}{\text{interfacial area}} = \frac{r_0}{3}$$

thus

$$r_0 = \frac{3}{\rho_{Si} S_a} \qquad (10)$$

An example of the fit (correlation coefficient 0.998) is shown in Fig. 14, with data taken from Fig. 9 for nitridation subsequent to the initial linear region (≈20% conv.) and ending at full conversion.

From the corresponding slopes, D_{eff} was calculated for the nitridation of 5–10 μm silicon at 1350, 1300, 1275, 1250 and 1200 °C, yielding the temperature dependency, assumed to be of the Arrhenius form $D_{eff} = D_0 \exp(-E_d/RT)$. Linearizing gives

$$\ln(D_{eff}) = \ln(D_0) - \left(\frac{E_d}{R}\right)\frac{1}{T} \qquad (11)$$

with the slope equal to E_d/R and the intercept equal to ln (D_0). Fig. 15 shows the plot of ln (D_{eff}) versus $1/T$, and indicates reasonably good correlation ($r = 0.984$) with the Arrhenius form, and furthermore, yields an activation energy, E_d, of 310.0 kJ mol^{-1}. Hence, D_{eff} can be expressed as

$$D_{eff} = 14.725 \exp\left(-\frac{310.0 \text{ kJ mol}^{-1}}{RT}\right)(\text{cm}^2 \text{s}^{-1}) \qquad (12)$$

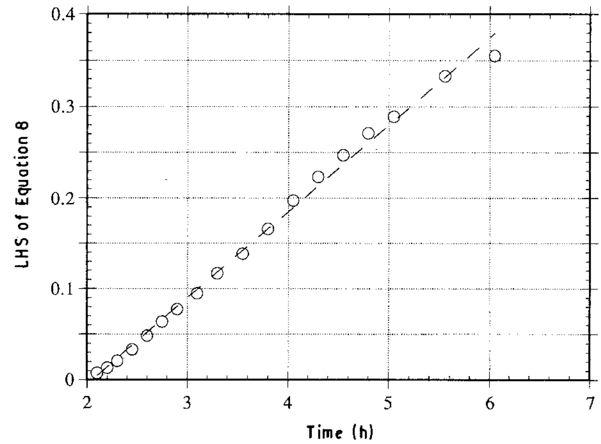

Figure 14 Least squares analysis for comparison of the intrinsic nitridation data at 1350 °C (from Fig. 9) with the sharp-interface model, incorporating Si_3N_4 product layer expansion, and subject to diffusional control. Of additional interest is the slope of the best fit line to obtain D_{eff}. Particle size = 5–10 μm.

which is on the order of 10^{-9}–10^{-10} cm^2 s^{-1} for typical nitridation temperatures.

Alternatively, the average dimension of the silicon fraction could be used for r_0 instead of the expression in Equation 10. In the case of the 5–10 μm fraction, this would imply $2r_0 = 7.5$ μm. When the aforementioned analysis for D_{eff} (T) is carried out in a similar

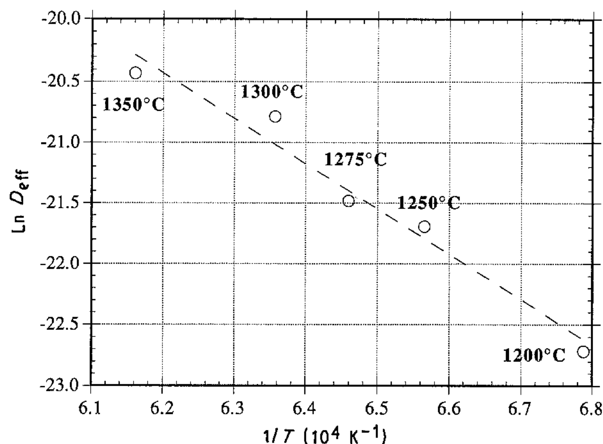

Figure 15 Plot of ln D_{eff} versus $1/T$ using the data from the SIM least squares analysis, indicating good correspondence to Arrhenius-type behaviour.

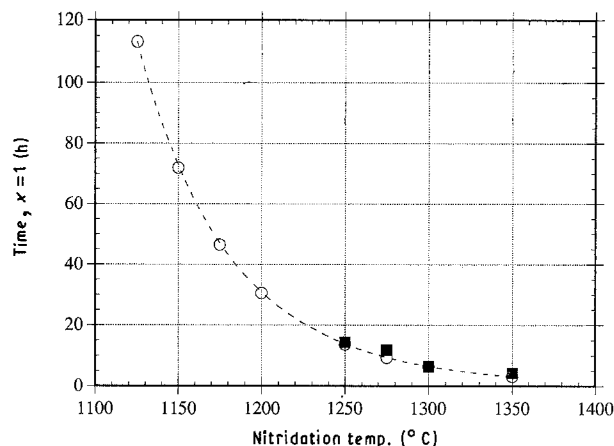

Figure 16 Comparison of the time required to achieve full conversion ($x = 1$) based on the sharp-interface model with 21.61% vol expansion (○). The experimental data shown (■) are intrinsic data (4.6 mg) for the nitridation of the 5–10 μm silicon (BET area $= 1.108\ \text{m}^2\ \text{g}^{-1}$).

manner, Equation 12 is altered to yield

$$D_{\text{eff}} = 153.34 \exp\left(-\frac{310.0\ \text{kJ mol}^{-1}}{RT}\right)(\text{cm}^2\ \text{s}^{-1}) \quad (13)$$

where D_{eff} is increased by approximately one order of magnitude to 10^{-8}–10^{-9} cm^2 s^{-1} with an unchanged E_{d}.

It is interesting to note that this activation energy, E_{d}, is in excellent agreement with the activation energy, E_{a}, obtained based on the intrinsic rate analysis (Equation 5), and is further evidence that the intrinsic behaviour is indeed diffusion-controlled through the Si_3N_4 product layer, and that the behaviour is well represented by the classical sharp-interface model with product layer expansion. It is also interesting to note the relative magnitude of D_{eff}, which is clearly below the Knudsen diffusion regime, but is many orders of magnitude larger than D_{eff} for polycrystalline α- or β-Si_3N_4. This is consistent with the idea that the individual silicon particles must expand by 21.6% during conversion to Si_3N_4, and hence, it is likely that microcracks develop in the Si_3N_4 product layer, allowing diffusion of nitrogen to reach the unreacted silicon core. Subsequent sintering and densification of this product layer occurs, and may be the reason why there appears to be an upper limit on the thickness of crystalline silicon that may be nitrided to full conversion, possibly on the order of 50 μm or so.

The SIM analysis can be extended to predict the time required to reach full conversion. Setting $x = 1$ in Equation 8 and substituting in Equation 12 for D_{eff} results in a relationship describing the time to attain full conversion as a function of particle radius and temperature

$$t(\text{h}) = 0.3553\left(\frac{r_0^2 \rho_{\text{Si}}}{7200\, \eta M_{\text{w}} C_{\text{N}_2}}\right) \times \left[\frac{1}{14.725 \exp(-37\,287/T)}\right] \quad (14)$$

where C_{N_2} is described by the ideal gas law. Using the data for the intrinsic behaviour of the 5–10 μm fraction (Fig. 9), the time to reach full conversion was plotted versus the nitridation temperature. For comparison, the theoretical curve based on Equation 14, and using Equation 10 for r_0, was also computed. The results are summarized in Fig. 16. When Equation 13 is used for D_{eff} instead, along with $r_0 = 3.75$ μm (average of the sieved size), essentially no difference is observed in the theoretical curve of Fig. 16. It is clear that a good match with the experimental data was achieved for temperatures ranging between 1250 and 1350 °C, values most commonly used in the nitridation process.

3.7. Description of the RBSN process

The nitridation of silicon to form a reaction-bonded compact is inherently complicated. The very nature of the process entails many aspects atypical of most ceramic systems such as the retention of the overall external dimensions of the compact while the individual silicon particles expand by 21.6% in volume during the reaction to form silicon nitride, suggesting that surface diffusion and vaporization–condensation type mechanisms are operative. Current understanding indicates that indeed such mechanisms are functional in the formation of the α-matte, α-whiskers, and β-spikes. During the RBSN process there is a dramatic decrease in macropore dimensions, which inhibits free diffusion of reacting species within the compact. Full conversion can be achieved, but not in conjunction with the absence of voids.

In spite of these complex details, the RBSN process can be divided into three fundamental stages, shown schematically in Fig. 17, each controlled by either intrinsic or global (compact) effects. For this general description, we make a distinction between the two effects by suggesting that any observations resulting from the basic process of nitrogen reacting with non-porous, polycrystalline silicon as being intrinsic in nature, while any observations resulting from the influence of adjacent particles, such as would be encountered in the nitridation of a compact or an excess quantity of free powder, as being global in nature. The

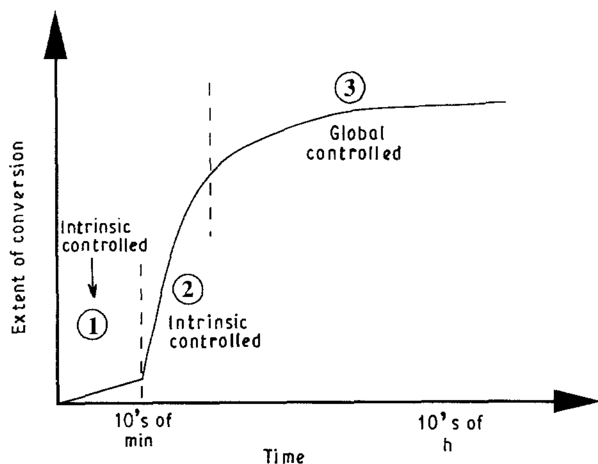

Figure 17 Schematic representation of the reaction-bonding process divided into three major stages: (1) initial nucleation/devitrification, (2) massive nitridation, and (3) final nitridation or termination.

terms are selected for ease of description. The following conclusions can be reached based on kinetic data and microstructural observations, as obtained in our experimental work and as reported in the literature.

During the initial stage (up to ~10%–15% conversion), silicon nitride nuclei form on the exposed silicon surface, this process being dominated by intrinsic effects, mainly the available surface area. These nuclei appear to have some type of a "seeding" effect whereby extensive nitridation is encouraged following this stage. This process is affected by pressure, with higher pressures resulting in a faster initial rate, probably due to its influence on the density of chemisorbed nitrogen [41]. However, its dependency on temperature is quite minor once the process has initiated, at least for temperatures between 1150 and 1350 °C as was shown by the early linear region in Fig. 9. Devitrification of the relatively impervious SiO_2 layer may be the controlling factor for this stage, as was suggested in Section 3.4. It is clear that diffusion of nitrogen to the inner regions of the compact is completely uninhibited, and hence, C_{N_2} is independent of radial position and remains at a constant value equal to the bulk concentration. During this stage, a truly homogeneous situation exists. This would not, however, apply to extremely high green densities or to the nitridation of ultrafine silicon, where the average macropore size may already be of the order of the mean free path of nitrogen.

The second stage represents the majority of nitridation (from 10% to 30%–90% or higher) resulting in pore filling and density increase, with temperature and surface area being the primary factors controlling the rate of this process. During the initial part of this stage, nitrogen is able to freely diffuse ($D_{eff} > 10^{-2}\ cm^2\ s^{-1}$) throughout the macropore structure. However, the permeability progressively decreases as the particles expand into the macropores. This is particularly significant for particles near the outer edge of the compact, resulting in a transition from binary to Knudsen diffusion ($D_{eff} \approx 10^{-2}$–$10^{-5} cm^2\ s^{-1}$), and eventually to diffusion characterized by transport of gas in relatively non-porous Si_3N_4 that has expanded into the interstitial space ($D_{eff} \ll 10^{-5}\ cm^2\ s^{-1}$). This latter form of gas transport is known as configurational diffusion [63], and results in a sharp kneeing in the kinetic data and the onset of the final stage. Nevertheless, the second stage is also controlled by intrinsic effects, i.e. molecular-hindered diffusion through the Si_3N_4 product layer forming on the individual silicon grains, as was shown in the SIM analysis of Section 3.6.

In the final stage of nitridation, the conversion versus time behaviour is dramatically slower. Compact effects dominate, typically manifest in the formation of a dense "watermelon-like" product layer on the outer edges of the compact, rendering full conversion difficult in large sample sizes. In many instances, full conversion is not attainable even though void fraction within the bulk of the compact remains relatively high. Under such circumstances, increasing the partial pressure of nitrogen or the nitridation temperature above the melting point of silicon may be the only viable means of completing the reaction. Table IV summarizes the three stages and indicates the controlling factors.

4. Conclusions

In the present work, careful attention was paid to minimizing extraneous contributions during silicon nitridation. In this light, gettered ultra-high purity gases, high-purity silicon, a molybdenum lined furnace tube, and molybdenum crucibles to hold the silicon were used, so that the sample was never in proximity with potential oxygen sources, and was effectively isolated from metallic impurity sources such as the ceramic furnace tube.

By careful selection of sample size, we obtained the intrinsic nitridation behaviour of strictly-defined fractions of silicon in the ranges of 5–10, 10–15, 15–20 and 20–37 μm under ultrapure conditions. The subsequent kinetic analysis has established an intrinsic rate equation (Equation 5) that is appropriate for all nitriding systems, indicating the maximum rate of reaction (mol Si reacted h^{-1}) that can be observed at a given temperature (K) and specific surface area ($m^2\ g^{-1}$). This equation can alternatively be expressed in units of % conv. h^{-1} (Equation 7). The rate parameters were determined by varying particle size (or surface area) at a constant temperature (1350 °C), and then varying temperature (between 1200 and 1350 °C) at a constant particle size (5–10 μm). An activation energy of 301.5 $kJ\ mol^{-1}$ was obtained, that is consistent with the values for diffusion of nitrogen through polycrystalline α-Si_3N_4 (233 $kJ\ mol^{-1}$) and β-Si_3N_4 (777 $kJ\ mol^{-1}$) [54]. Furthermore, its value is closer to that of the α-phase, which is consistent with the high α/β phase ratio typically obtained in the nitridation of high-purity silicon below its melting point (1413 °C).

Further kinetic analysis has established that the process is intrinsically controlled by diffusional limitations through the Si_3N_4 product layer developing on the individual silicon grains. The rate of chemical reaction at the Si–Si_3N_4 interface and diffusion through the external boundary layer appear to be much faster, and hence, are not a factor in the rate

TABLE IV Summary of the factors affecting the three fundamental stages of the RBSN process. Macroscopic porosity refers to the voids between adjacent silicon particles, while microscopic porosity refers to the permeability within the Si_3N_4 product layer forming on the individual silicon grains

Stage	Main processes	Intrinsic effects	Global (compact) effects	Controlling factors
1.	(a) Devitrification (b) Initial nucleation	(a) $R_i = f(P_{N_2}, S_a) \neq f(T)$ (weak dependency)	(a) Binary diffusion through macropores (b) C_{N_2} in macropores = bulk conc. = constant	Intrinsic
2.	(a) Nucleation (b) Surface diffusion (c) Vaporization–condensation	(a) $R_i = f(P_{N_2}, S_a, T)$ (b) Diffusion through the developing Si_3N_4 product layer (micropores) following Eq 12	(a) Binary diffusion through macropores initially dominant (b) Decrease in macroscopic permeability developing into controlling factor (c) Knudsen diffusion through macropores increasingly important	Intrinsic
3.	Any available mechanism	(a) Diffusion in micropores increasingly impeded due to densification of product layer. Limits maximum Si grain size that can be nitrided to completion (b) Configurational diffusion through any available pathway	(a) Knudsen diffusion through macropores ending. "Kneeing" in conv. versus time curve occurs (b) Configurational diffusion becoming dominant (c) N_2 diffusion markedly impeded. Full conversion difficult	Global

determining step. A sharp-interface model was established (Equation 8), that incorporates the effects of product layer expansion. This equation allows for the determination of D_{eff} through the Si_3N_4 product layer (Equation 12), with its value being well below the Knudsen diffusion regime (10^{-2}–10^{-5} $cm^2 s^{-1}$) as expected. Additionally, its activation energy was determined to be essentially the same as the value obtained in the earlier intrinsic data analysis, yielding further supporting evidence to the validity of both these analyses.

This work, in conjunction with other recent studies (e.g. [64]), provides the fundamental basis for the future development of a complete, structural model of the reaction-bonding process, that incorporates competing features, namely particle sintering and nitride formation, and also includes the effects of particle size, particle packing, and thermal and concentration gradients. Additional features of importance include the expansion of the individual grains during compact nitridation while maintaining overall external dimensions, and the ability to predict a priori the α/β phase ratio and the conversion versus time behaviour as a function of particle size, temperature, and green density. Such a model would be instrumental in providing the basis for future experiments, optimizing industrial nitriding schedules, and advancing the current understanding of the reaction-bonding process.

Our conclusions are as follows.

1. The vast majority of the published nitridation data involves contributions tractable to global effects, such as compact formation, and hence, fails to isolate intrinsic behaviour. As a result, a wide range of possible models has been reported in the literature, each applicable only for a specific set of nitridation conditions.

2. Silicon vaporization rates at nitriding temperatures are more than enough to validate the observed reaction rates, indicating the importance of $3\,Si_{(g)} + 2\,N_{2(g)} \rightarrow Si_3N_{4(s)}$ as a major contributor to the nitridation process.

3. Low-density compacts nitride in the initial stages following true intrinsic behaviour, where the maximum rate observed is identical to the maximum intrinsic rate. However, this behaviour is short-lived as compact permeability decreases causing macroscopic nitrogen gradients to develop. "Kneeing" in the conversion versus time behaviour is observed.

4. The initial intrinsic rate (i.e. the maximum rate observed) is strongly dependent on the temperature of nitridation and the surface area available for nucleation and silicon vaporization. The experimentally determined activation energy of 301.5 kJ mol^{-1} corresponds to diffusional limitation in the developing Si_3N_4 product layer with a high α/β phase ratio.

5. The nitridation kinetics for the overall conversion of an individual grain of silicon follow a sharp-interface model with 21.6 vol % product layer expansion. The Si_3N_4 product layer that subsequently develops restricts free nitrogen diffusion to the unreacted silicon core. Reaction at the Si–Si_3N_4 interface and diffusion through the external boundary layer are

faster than the diffusion of nitrogen through the product layer, and hence, are not rate determining. The temperature dependence of D_{eff} was established, with its activation energy comparing favourably with that for the intrinsic rate.

6. The nitridation of silicon compacts to form reaction-bonded bodies can be viewed to occur in three fundamental stages: (1) initial devitrification/nucleation, (2) massive nitridation, and (3) termination. The first two stages are controlled by intrinsic effects, and hence, are invariant with respect to all nitriding systems, while the latter is controlled by global or compact effects due to closure of the macropores.

Acknowledgements

One of the authors (RGP) gratefully acknowledges the award of a Graduate Assistance in the Area of National Needs (GAANN) Fellowship, under the auspices of the Center for Bioengineering and Pollution Control at the University of Notre Dame, during the course of this study. We also thank Professor D. Ramkrishna, Purdue University, for use of the Quantimet 570 particle size analyser.

References

1. H. LANGE, G. WÖTTING and G. WINTER, *Angew. Chem. Int. Ed. Engl.* **30** (1991) 1579.
2. F. L. RILEY, *Mater. Sci. Forum* **47** (1989) 70.
3. H. M. JENNINGS, B. J. DALGLEISH and P. L. PRATT, *J. Mater. Sci.* **23** (1988) 2573.
4. G. ZIEGLER, J. HEINRICH and G. WÖTTING, *ibid.* **22** (1987) 3041.
5. H. M. JENNINGS, *ibid.* **18** (1983) 951.
6. A. J. MOULSON, *ibid.* **14** (1979) 1017.
7. M. E. WASHBURN and W. S. COBLENZ, *Bull. Amer. Ceram. Soc.* **67** (1988) 356.
8. A. ATKINSON, P. J. LEATT and A. J. MOUSLON, *Proc. Brit. Ceram. Soc.* **22** (1973) 253.
9. J. A. MANGELS, *Bull. Amer. Ceram. Soc.* **60** (1981) 613.
10. P. WONG and D. R. MESSIER, *ibid.* **57** (1978) 525.
11. M. MITOMO, *J. Mater. Sci.* **12** (1977) 273.
12. S.-S. LIN, *J. Amer. Ceram. Soc.* **60** (1977) 78.
13. *Idem, ibid.* **61** (1978) 95.
14. S. M. BOYER and A. J. MOULSON, *J. Mater. Sci.* **13** (1978) 1637.
15. W. A. FATE and M. E. MILBERG, *J. Amer. Ceram. Soc.* **61** (1978) 531.
16. D. CAMPOS-LORIZ, S. P. HOWLETT, F. L. RILEY and F. YUSAF, *J. Mater. Sci.* **14** (1979) 2325.
17. J. MUKERJI and S. K. BISWAS, *J. Amer. Ceram. Soc.* **64** (1981) 549.
18. J. R. G. EVANS and A. J. MOULSON, *J. Mater. Sci.* **18** (1983) 3721.
19. C. E. BOULDIN, E. A. STERN, M. S. DONLEY and T. G. STOEBE, *ibid.* **20** (1985) 1807.
20. W. R. MOSER, D. S. BRIERE, R. CORREIA and G. A. ROSSETTI, *J. Mater. Res.* **1** (1986) 797.
21. R. G. PIGEON, A. VARMA and A. E. MILLER, *J. Mater. Sci.* (1993) in press.
22. R. B. GUTHRIE and F. L. RILEY, *J. Mater. Sci. Lett.* **9** (1974) 1363.
23. D. CAMPOS-LORIZ and F. L. RILEY, *ibid.* **11** (1976) 195.
24. J. A. MANGELS, *J. Amer. Ceram. Soc.* **58** (1975) 354.
25. D. P. ELIAS and M. W. LINDLEY, *J. Mater. Sci.* **11** (1976) 1278.
26. B. F. JONES and M. W. LINDLEY, *ibid.* **11** (1976) 1969.
27. W. M. DAWSON and A. J. MOULSON, *J. Mater. Sci. Lett.* **13** (1978) 2289.
28. M. W. LINDLEY, D. P. ELIAS, B. F. JONES and K. C. PITMAN, *J. Mater. Sci.* **14** (1979) 70.
29. D. CAMPOS-LORIZ and F. L. RILEY, *J. Mater. Sci. Lett.* **14** (1979) 1007.
30. H. DERVISBEGOVIC and F. L. RILEY, *ibid.* **14** (1979) 1265.
31. *Idem, J. Mater. Sci.* **16** (1981) 1945.
32. N. J. SHAW, *J. Mater. Sci. Lett.* **1** (1982) 337.
33. H. KIM and C. H. KIM, *ibid.* **3** (1984) 199.
34. *Idem, ibid.* **3** (1984) 201.
35. *Idem, ibid.* **3** (1984) 203.
36. *Idem, J. Mater. Sci.* **20** (1985) 141.
37. *Idem, ibid.* **20** (1985) 149.
38. M. N. RAHAMAN and A. J. MOULSON, *ibid.* **19** (1984) 189.
39. B. F. JONES and M. W. LINDLEY, *ibid.* **11** (1976) 1288.
40. K. J. HEUTTINGER, *High Temp. High Press.* **1** (1969) 221.
41. A. ATKINSON, A. J. MOULSON and E. W. ROBERTS, *J. Amer. Ceram. Soc.* **59** (1976) 285.
42. H. M. JENNINGS and M. H. RICHMAN, *J. Mater. Sci.* **11** (1976) 2087.
43. A. VARMA, R. G. PIGEON and A. E. MILLER, *ibid.* **26** (1991) 4541.
44. D. S. THOMPSON and P. L. PRATT, in "Science of Ceramics", Vol. 3, edited by G. H. Stewart (Academic Press, New York, 1967) p. 33.
45. D. R. MESSIER and P. WONG, *J. Amer. Ceram. Soc.* **56** (1973) 480.
46. M. I. MENDELSON, *J. Mater. Sci. Lett.* **14** (1979) 1752.
47. R. G. PIGEON and A. VARMA, *ibid.* **11** (1992) 1370.
48. I. LANGMUIR, *Phys. Rev.* **5** (II) (1913) 329.
49. O. J. GREGORY, S.-B. LEE and R. C. FLAGAN, *J. Amer. Ceram. Soc.* **70** (1987) C-52.
50. K. ISHIZAKI, S. YUMOTO and K. TANAKA, *J. Mater. Sci.* **23** (1988) 1813.
51. *Idem, ibid.* **24** (1989) 3553.
52. W. SYMONS, K. J. NILSEN and S. C. DANFORTH, in "Ultrastructure Processing of Advanced Ceramics", edited by J. D. Mackenzie and D. R. Ulrich (Wiley, New York, 1988) p. 907.
53. A. ATKINSON, A. J. MOULSON and E. W. ROBERTS, *J. Mater. Sci. Lett.* **10** (1975) 1242.
54. K. KIJIMA and S. SHIRASAKI, *J. Chem. Phys.* **65** (1976) 2668.
55. L. K. DORAISWAMY and M. M. SHARMA, "Heterogeneous Reactions: Analysis, Examples, and Reactor Design", Vol. 1 (Wiley, New York, 1984) p. 450.
56. J. SZEKELY, J. W. EVANS and H. Y. SOHN, "Gas-Solid Reactions" (Academic Press, New York, 1976) p. 65.
57. S. F. HULBERT, *J. Brit. Ceram. Soc.* **6** (1969) 11.
58. R. B. GUTHRIE and F. L. RILEY, *Proc. Brit. Ceram. Soc.* **22** (1973) 275.
59. B. J. DALGLEISH, H. M. JENNINGS and P. L. PRATT, *ibid.* **31** (1981) 85.
60. O. J. GREGORY and M. H. RICHMAN, *Metallogr.* **15** (1982) 157.
61. H. M. JENNINGS, B. J. DALGLEISH and P. L. PRATT, *J. Mater. Sci.* **23** (1988) 2573.
62. R. ARIS, "The Mathematical Theory of Diffusion and Reaction in Permeable Catalysts", Vol. 1 (Clarendon Press, Oxford, 1975).
63. G. F. FROMENT and K. B. BISCHOFF, "Chemical Reactor Analysis and Design", 2nd Edn (Wiley, New York, 1990) p. 142.
64. W. KU, O. J. GREGORY and H. M. JENNINGS, *J. Amer. Ceram. Soc.* **73** (1990) 286.

Received 27 April
and accepted 12 October 1992